Medical Engineering and Physics 38 (2016) 1131–1135

Contents lists available at ScienceDirect

Medical Engineering and Physics

journal homepage: www.elsevier.com/locate/medengphy

Technical note

Accuracy of model-based tracking of knee kinematics and cartilage contact measured by dynamic volumetric MRI

Jarred Kaiser[a], Arezu Monawer[a], Rajeev Chaudhary[b], Kevin M. Johnson[c], Oliver Wieben[b,c], Richard Kijowski[d], Darryl G. Thelen[a,b,e,*]

[a] Department of Mechanical Engineering, University of Wisconsin - Madison, 1415 Engineering Drive, Madison, WI 53706, USA
[b] Department of Biomedical Engineering, University of Wisconsin - Madison, 1415 Engineering Drive, Madison, WI 53706, USA
[c] Department of Medical Physics, University of Wisconsin - Madison, 1111 Highland Avenue, Madison, WI 53705, USA
[d] Department of Radiology, University of Wisconsin - Madison, 600 Highland Avenue, Madison, WI 53792, USA
[e] Department of Orthopedics and Rehabilitation, University of Wisconsin - Madison, 1685 Highland Avenue, Madison, WI 53705, USA

ARTICLE INFO

Article history:
Received 8 September 2015
Revised 7 May 2016
Accepted 8 June 2016

Keywords:
Dynamic MRI
Knee kinematics
Validation
Biomechanics

ABSTRACT

The purpose of this study was to determine the accuracy of knee kinematics and cartilage contact measured by volumetric dynamic MRI. A motor-actuated phantom drove femoral and tibial bone segments through cyclic 3D motion patterns. Volumetric images were continuously acquired using a 3D radially undersampled cine spoiled gradient echo sequence (SPGR-VIPR). Image data was binned based on position measured *via* a MRI-compatible rotary encoder. High-resolution static images were segmented to create bone models. Model-based tracking was performed by optimally registering the bone models to the volumetric images at each frame of the SPGR-VIPR series. 3D tibiofemoral translations and orientations were reconstructed, and compared to kinematics obtained by tracking fiducial markers. Imaging was repeated on a healthy subject who performed cyclic knee flexion-extension. Cartilage contact for the subject was assessed by measuring the overlap between articular cartilage surfaces. Model-based tracking was able to track tibiofemoral angles and translations with precisions less than 0.8° and 0.5 mm. These precisions resulted in an uncertainty of less than 0.5 mm in cartilage contact location. Dynamic SPGR-VIPR imaging can accurately assess *in vivo* knee kinematics and cartilage contact during voluntary knee motion performed in a MRI scanner. This technology could facilitate the quantitative investigation of links between joint mechanics and the development of osteoarthritis.

1. Introduction

Magnetic resonance imaging (MRI) is an attractive modality for investigating the effects of osteoarthritis (OA) on cartilage tissue. High resolution MRI can track localized changes in cartilage thickness associated with the progression of OA [1–4]. In addition, compositional changes in cartilage, which arise before the onset of cartilage thinning, can be monitored using quantitative MRI techniques [5–7]. However, these static imaging protocols cannot provide insights into the underlying cartilage tissue loading patterns, which are theorized to contribute to the development and progression of OA [8,9].

Dynamic MR imaging sequences can potentially fill this void by providing a mechanism to assess joint kinematics [10–13] and associated cartilage contact patterns [6,14]. Unfortunately, the relatively slow acquisition rate of MRI makes real-time 3D imaging of dynamic joint motion challenging [15,16]. Alternatively, cine imaging sequences are often used to accumulate images over repeat motion cycles [12,17–19]. The most common dynamic MRI sequence used for skeletal motion tracking is cine phase contrast (cine-PC) imaging. Cine-PC provides a measure of 3D skeletal velocities that can be integrated to estimate joint position and orientation [11,14,17,20]. However, integration of imprecise velocity information can contribute to bias errors in segment position and orientation [21,22], which has adverse effects on the accuracy of cartilage contact calculations.

We recently introduced a new dynamic cine MRI sequence, termed SPoiled-GRadient echo with Vastly under-sampled Isotropic PRojection imaging (SPGR-VIPR), which uses radially undersampled isotropic trajectories to obtain fully 3D anatomical images of the knee during cyclic movement [12]. Subject-specific models of bone and cartilage morphology are separately segmented from high resolution static images. Model-based tracking is then performed by

* Corresponding author at: Department of Mechanical Engineering, University of Wisconsin - Madison, 1415 Engineering Drive, Madison, WI 53706, USA.
Tel.: +1 608 262 1902; fax: +1 608 265 2316.
E-mail address: dgthelen@wisc.edu (D.G. Thelen).

http://dx.doi.org/10.1016/j.medengphy.2016.06.016
1350-4533/

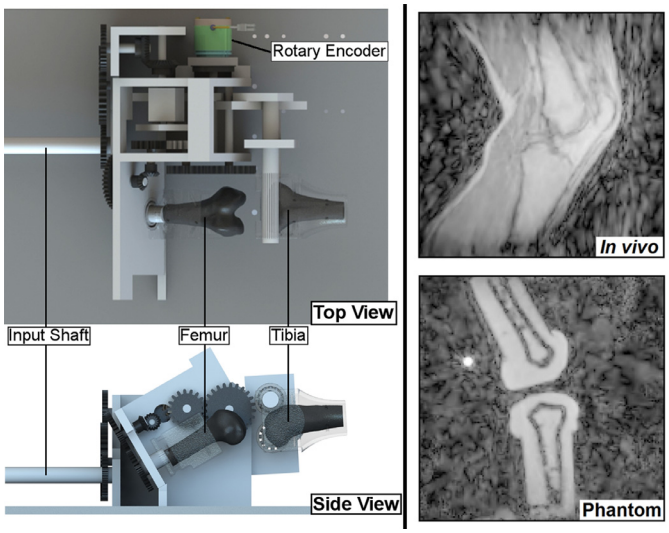

Fig. 1. (Left) A stepper motor located outside the MRI bore drives the input shaft of the motion phantom, generating cyclic motion of the tibial and femoral bone segments. (Right) Dynamic SPGR-VIPR images obtained during voluntary *in vivo* motion and motor-actuated phantom motion. The bright spot posterior to the femur in the phantom image is a fiducial marker.

registering the bone models to the volumetric SPGR-VIPR images at each time frame. A detailed characterization of the cartilage contact patterns is obtained by assessing the proximity between articular cartilage surfaces. Contact data can then be compared to measures of cartilage morphology and composition, providing insights into the potential mechanical precipitators of OA [6].

The purpose of the presented work was twofold. First, we used a motion phantom to determine the accuracy of using SPGR-VIPR to track 3D joint kinematics. Second, we used SPGR-VIPR scans of voluntary knee movement to assess the sensitivity of cartilage contact to potential errors in skeletal kinematics. Completion of these aims provides an estimate of the accuracy with which cartilage contact can be inferred from SPGR-VIPR images.

2. Materials and methods

We constructed a MR-compatible motion phantom to cyclically move femoral and tibial bone segments over ranges of motion that mimic natural knee behavior (Fig. 1). The motion phantom uses a seven-bar linkage system (similar to that used by Smith [23]) and a series of gears to convert a continuous rotary input into femoral internal rotation and tibial flexion. Bone segments, based on the geometry of a healthy young female (23 years, 1.65 m, 61 kg), were 3D printed out of ABS plastic and then embedded in an agar gel with MR relaxation parameters comparable to muscle tissue [24]. Embedded bone segments were rigidly secured to the motion phantom. Four ellipsoidal vitamin E pills (major/minor diameters: 15/10 mm), acting as fiducial markers, were secured to each bone segment to allow for an independent assessment of skeletal kinematics.

The motion phantom was placed into the bore of a clinical 3.0 T MR scanner (MR750, General Electric Healthcare, Waukesha, WI). A 16-channel flex coil (GEM Flex, NeoCoil, Pewaukee, WI) was placed over the motion volume. The phantom was actuated by a continuously rotating 2-phase stepper motor (83-62, Parker Hannifin Corp, Rohnert Park, CA) controlled *via* ministep drive (Parker/Digiplan PDX 13, Parker Hannifin Corp, Rohnert Park, CA). The bone segments were driven at a rate of 0.5 Hz, with the tibia rotating through $31.7 \pm 0.7°$ of flexion and the femur rotating $12.0 \pm 0.4°$ about its long axis. A MR-compatible rotary encoder (MR310, Micronor, Newbury Park, CA), mounted on the phantom, was used to delineate motion cycles within the scanner (Fig. 1).

A high-resolution static IDEAL SPGR sequence ($0.37 \times 0.37 \times 0.9\,mm^3$ resolution, TR/TE= 10.5/2.2 ms) was first acquired of the phantom in a fixed position. Models of the femur and tibia were created by manually segmenting (MIMICS, Materialize Group, Leuven, Belgium) these images. We then collected continuous dynamic SPGR-VIPR images ($1.5 \times 1.5 \times 1.5\,mm^3$ acquired spatial resolution, TR/TE = 4 ms/1.4 ms, flip angle = 8°, BW= 62.5 kHz, FOV= $24 \times 24 \times 24\,cm^3$, 75,000 unique radial lines) of the actuated phantom over five minutes. Dynamic images were reconstructed by using the rotary encoder to retrospectively sort the acquired projections into 60 image frames with no view sharing [12]. Three unique trials were sequentially collected during the same imaging session.

The position and orientation of the bone segments were measured in each frame of the dynamic MR series using two independent techniques. We first used a model-based tracking technique, the details of which can be found in [12]. Briefly, bone models were optimally registered to each dynamic image frame to find the 3D bone pose that minimized the sum of squared intensities of the dynamic image at the locations of the model vertices. This function drives the bone models to the low-intensity outlines seen in the dynamic images (Fig. 1). We separately used the fiducial markers to measure kinematics by applying a threshold to the dynamic images such that the bright fiducials remained visible without surrounding signal noise. A spherical search region (radius = 2 cm) was initialized at the center of each fiducial. The centers of each fiducial in sequential frames were then automatically determined by calculating the average location of pixels within the search region weighted by their intensities. The static images were used to establish the location of each fiducial within the anatomical bone reference frames. We then used a singular value decomposition approach to determine the bone pose that optimally fit the bones to the fiducial marker positions [25].

Tibiofemoral kinematics were characterized as the translation and orientation of the tibia segment relative to the femur segment. Kinematics were low-pass filtered with a 5 Hz cutoff frequency. Error for the fiducial-based tracking was calculated as the standard deviation of the inter-fiducial distance averaged over the three trials. Accuracy of the model-based tracking was characterized by bias (average difference between tracked kinematics), precision (standard deviation of differences) and root mean squared (RMS) error metrics. All metrics were averaged over the three repeat trials.

Static IDEAL SPGR and dynamic SPGR-VIPR images were also acquired on a healthy female subject (18 years, 66 kg, 165 cm), who gave informed written consent for the IRB-approved protocol. IDEAL SPGR images were first collected with the subject's knee extended within an eight-channel phased-array extremity coil (Invivo, Orlando, FL) and segmented to obtain models of the femur and tibia. A FSE Cube sequence ($0.31 \times 0.31 \times 1\,mm^3$ resolution, TR/TE= 2066.7/19.7 ms) was segmented to obtain the femoral and tibial articular cartilage geometries. For dynamic imaging, the subject laid supine on an MR-compatible knee loading device [12] with a 16-channel wrap coil centered around the knee. The subject was asked to cyclically flex and extend her knee through ~35° of motion against an inertial load at 0.5 Hz for 5 min. SPGR-VIPR images were reconstructed into 60 frames. Model-based tracking was used to determine tibiofemoral kinematics. We initialized the optimization routine with random segment positions and orientations (±2 mm and ±2° from the nominal case) and repeated the optimal bone tracking ten times to evaluate the repeatability.

To assess contact, we registered cartilage geometries to the bone models at each frame of the motion cycle. We calculated

Table 1
Bias, precision, and root-mean squared error of model-based tracking of dynamic SPGR-VIPR images.

	Tibiofemoral angles (°)			Tibiofemoral translations (mm)		
	Flexion	Adduction	Int. rot.	Lateral	Anterior	Superior
Bias	0.03 ± 0.05	0.68 ± 0.09	0.21 ± 0.08	0.04 ± 0.03	0.19 ± 0.05	0.46 ± 0.06
Precision	0.47 ± 0.02	0.81 ± 0.12	0.69 ± 0.16	0.47 ± 0.08	0.23 ± 0.05	0.24 ± 0.03
RMS Error	0.47 ± 0.01	1.06 ± 0.13	0.72 ± 0.12	0.60 ± 0.08	0.30 ± 0.03	0.52 ± 0.06

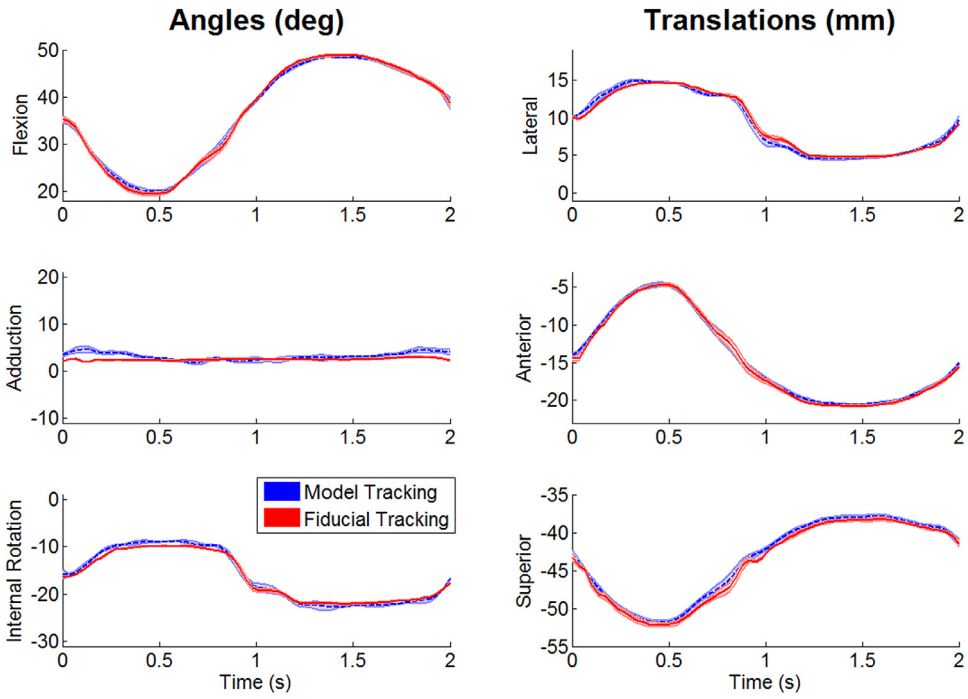

Fig. 2. Angular and translational kinematics of the tibia relative to the femur in the motion phantom. Good temporal agreement is seen between kinematic trajectories obtained using model-based and fiducial tracking algorithms.

the proximity between the femoral and tibial cartilage surfaces for each face in the tibial cartilage surface mesh. Center of contact was defined as the weighted-average position of the contact region on the tibia, with the position of each mesh face weighted by its proximity metric. Kinematics were then varied by 0.1 mm or 0.1° at every 5° of knee flexion to determine the sensitivity of measured cartilage contact location and area to joint translations and orientation angles. Sensitivities were independently computed at each image frame and then averaged over all 60 frames of the motion cycle. To determine the uncertainty in cartilage contact metrics from tracked kinematics, we multiplied the average sensitivities by the precision of the model-based tracking.

3. Results

Fiducial-based tracking of the motion phantom resulted in inter-fiducial distance errors of 0.16 mm in the medial, anterior, and superior directions for the femur. Inter-fiducial distance errors were slightly larger for the tibia, averaging 0.20 mm, 0.19 mm, and 0.18 mm in the medial, anterior, and superior directions.

Relative to fiducial marker tracking of joint kinematics, model-based tracking was able to measure tibiofemoral flexion with an average bias of 0.03°, a precision of 0.47° and a RMS error of 0.47°. Tibiofemoral internal rotation was measured with an average bias of 0.21°, a precision of 0.69° and a RMS error of 0.72° (Table 1, Fig. 2). All three tibiofemoral translations were tracked with precisions less than 0.5 mm (Table 1).

Model-based tracking of the *in vivo* case was highly repeatable with standard deviations of less than 0.02° and 0.01 mm over ten repeat optimization solutions. The anterior–posterior center of contact was most sensitive to errors in sagittal plane angles and translations, whereas the medio–lateral center of contact was sensitive to errors in lateral tibia translation and tibiofemoral adduction (Table 2). Contact area exhibited the greatest sensitivity to errors in superior tibia translation and tibiofemoral adduction.

When combined with kinematic precision metrics, an uncertainty of < 0.50 mm in medial–lateral center of contact could arise from errors in tibiofemoral adduction and lateral translation (Table 3). Uncertainty in anterior–posterior center of contact ranged from 0.04 to 0.25 mm, with the greatest uncertainty associated with errors in tracked tibiofemoral flexion. Imprecision in tibiofemoral adduction and superior tibia translation resulted in a medial contact area uncertainty of 56 mm^2 and 36 mm^2, respectively.

4. Discussion

We recently introduced a novel 3D dynamic imaging protocol (SPGR-VIPR) for tracking *in vivo* joint motion, which addresses some of the challenges with prior dynamic MRI techniques such as phase contrast imaging [11,14,20,26]. This study showed that SPGR-VIPR images can reconstruct joint kinematics with a reasonably high precision, averaging less than 0.5 mm and 0.8°. The achieved kinematic precisions are smaller than asymmetric variations in kinematics seen in ACL-deficient [27] and –reconstructed

Table 2
Sensitivity of contact measures, including center of contact (CoC) and contact area, to variations in tibiofemoral angles and translations.

		Angles (per °)			Translations (per mm)		
		Flexion	Adduction	Int. rot	Lateral	Anterior	Superior
Medial CoC (mm)	**Medial**	0.10 ± 0.07	0.60 ± 0.09	0.19 ± 0.15	1.06 ± 0.10	0.18 ± 0.16	0.17 ± 0.15
	Lateral	0.03 ± 0.02	0.52 ± 0.06	0.11 ± 0.08	0.99 ± 0.14	0.10 ± 0.04	0.28 ± 0.01
Anterior CoC (mm)	**Medial**	0.53 ± 0.09	0.05 ± 0.05	0.32 ± 0.10	0.12 ± 0.06	0.58 ± 0.20	0.59 ± 0.27
	Lateral	0.29 ± 0.05	0.05 ± 0.04	0.19 ± 0.03	0.09 ± 0.04	0.43 ± 0.03	0.36 ± 0.11
Contact area (mm^2)	**Medial**	21.2 ± 13.8	68.6 ± 43.3	22.2 ± 18.1	36.7 ± 20.4	42.0 ± 31.0	149.8 ± 80.3
	Lateral	15.5 ± 9.4	24.3 ± 14.6	10.8 ± 6.7	40.4 ± 12.6	29.8 ± 22.5	106.7 ± 25.6

Table 3
Estimated uncertainty in cartilage contact metrics, including center of contact (CoC) and contact area, due to errors in tracking tibiofemoral kinematics.

		Tibiofemoral angles			Tibiofemoral translations		
		Flexion	Adduction	Int. rot	Lateral	Anterior	Superior
Medial CoC (mm)	**Medial**	0.05	0.49	0.13	0.49	0.04	0.04
	Lateral	0.01	0.43	0.08	0.46	0.02	0.07
Anterior CoC (mm)	**Medial**	0.25	0.04	0.22	0.06	0.13	0.14
	Lateral	0.14	0.04	0.13	0.04	0.10	0.09
Contact area (mm^2)	**Medial**	9.97	55.88	15.25	17.07	9.50	35.75
	Lateral	7.32	19.82	7.45	18.82	6.74	25.48

knees [28,29], such that SPGR-VIPR may be viable to detect clinically relevant abnormalities in knee mechanics.

Our kinematic tracking accuracy is comparable to that measured with biplane fluoroscopy. For example, a prior study of model-based tracking using biplane fluoroscopic images reported tibiofemoral kinematic precisions of 0.7 mm for translations and 0.9° for rotation angles [10]. It is noted that fluoroscopy has the advantage of being able to allow for high frame rate collections during functional activities such as running and jumping [29,30]. In addition, kinematic information from biplane fluoroscopy can be coupled with cartilage models derived from MRI to assess cartilage contact [31,32]. However, fluoroscopic approaches are reliant on specialized equipment and expose subjects to ionizing radiation, which makes it challenging to employ for large-scale and longitudinal clinical studies.

The most common dynamic MRI approach for tracking 3D skeletal motion uses cine phase contrast (cine-PC) imaging. Cine-PC imaging provides 3D bone velocity information, which can be numerically integrated to obtain bone pose throughout a cyclic motion task [11,20]. Validation studies have reported cine-PC MRI has an accuracy of 0.97°/0.33 mm for tracking skeletal motion [33], though these values do not include potential registration errors that can arise from fitting 3D bone models to planar images. Sequential static imaging provides similar accuracies for patellar kinematics (1.02°/0.88 mm [34]). However, static imaging cannot capture the dynamic muscle and inertial effects that arise in active motion and affect joint mechanics [15]. Multi-slice dynamic imaging has been proposed to supplant sequential static imaging [15]. However, real-time implementations of multi-slice imaging are currently only viable for slow, quasi-static motion.

Dynamic MR images can be co-registered with high resolution static images to assess cartilage contact in joint movement. This coupling is needed because dynamic images lack the resolution ($1.5 \times 1.5 \times 1.5\,mm^3$) necessary to delineate thin cartilage structures (2–5 mm [35]) seen in the knee. Similar to prior studies [6,14,31,32], we assessed contact by segmenting the unloaded cartilage tissue in high resolution images, registering the cartilage models to the bone models tracked in dynamic images and then quantifying the amount of overlap between cartilage surfaces. Based on the results of this study, we estimate that this method can estimate the center of cartilage contact to within 0.5 mm, with the greatest errors associated with the frontal plane joint angles and translations. Cartilage contact area uncertainties ranged up to 56 mm^2, which would represent ~15% of the medial tibiofemoral contact area measured in cadaveric knees [36]. These results suggest that while the current model-based tracking errors would allow an accurate assessment of the center of contact, further improvements in tracking may be necessary to accurately determine subtle changes in contact area. Ultimately, contact information is important for understanding the loading and deformation that cartilage tissue undergoes *in vivo*. To this end, MRI-based displacement encoding sequences have been recently introduced to assess *in vivo* cartilage tissue strain under cyclic compressive loading conditions [35,37,38].

There are limitations in the current study that are important to understand while interpreting our results. Similar to other studies [10,33], we relied on fiducial markers to assess the validity of our model-based tracking technique. The precision of tracking fiducial markers was 0.2 mm, which is nearly twice the precision of our model-based tracking. Ideally, the kinematic standard would provide approximately ten times greater precision than the technique being evaluated. This gold standard is difficult to achieve in dynamic imaging situations. Second, our cine imaging technique requires repeatable cyclic movement. In separate motion analyses of the phantom, the device generated 31.7 ± 0.7° of tibia flexion and 12.0 ± 0.4° of femoral rotation over 450 motion cycles. These excursions are comparable to the average ranges of knee motion (flexion = 37.1°, tibia rotation = 10.6°) and inter-cycle standard deviations (0.8°) we observed when using SPGR-VIPR to track knee kinematics in ten healthy young adults [12]. Thus, the phantom variability reasonably represented the variability seen *in vivo*. Finally, the wall thickness (5–7 mm) of the fabricated bone geometries exceeds the cortical bone thickness we see in human bone segments (Fig. 1). This discrepancy may slightly degrade the accuracy of our bone fitting algorithm, where bone models have greater leeway when registered to the thick, low signal bone edges visible in the phantom images.

In conclusion, model-based tracking of dynamic, 3D SPGR-VIPR images is capable of measuring tibiofemoral kinematics with a precision of less than one degree in rotation and less than 0.5 mm in

translation. This precision facilitates reasonably accurate estimates in the location of *in vivo* tibiofemoral cartilage contact. Hence, 3D SPGR-VIPR provides a powerful new approach for empirically examining potential links between abnormal cartilage contact patterns and the development of osteoarthritis.

Conflict of interest statement

The authors have no conflict of interest to disclose.

Acknowledgments

The authors gratefully acknowledge the funding provided by the NIH (EB015410, AR062733) and the contributions of Michael Vignos, James Hermus, Rob Bradford, Jonathon Mantes, David Bunger, and Kelli Hellenbrand.

Reference

[1] Burgkart R, Glaser C, Hyhlik-Dürr A, Englmeier KH, Reiser M, Eckstein F. Magnetic resonance imaging–based assessment of cartilage loss in severe osteoarthritis: Accuracy, precision, and diagnostic value. Arthritis Rheum 2001;44:2072–7.
[2] Frobell RB. Change in cartilage thickness, posttraumatic bone marrow lesions, and joint fluid volumes after acute ACL disruption. J Bone Jt Surg Am Vol 2011;93:1096–103.
[3] Eckstein F, Cicuttini F, Raynauld J-P, Waterton J, Peterfy C. Magnetic resonance imaging (MRI) of articular cartilage in knee osteoarthritis (OA): morphological assessment. Osteoarthr Cartil 2006;14:46–75.
[4] Calvo E, Palacios I, Delgado E, Ruiz-Cabello J, Hernandez P, Sanchez-Pernaute O, et al. High-resolution MRI detects cartilage swelling at the early stages of experimental osteoarthritis. Osteoarthr Cartil 2001;9:463–72.
[5] Liu F, Chaudhary R, Hurley SA, Rio A, Alexander AL, Samsonov A, et al. Rapid multicomponent T2 analysis of the articular cartilage of the human knee joint at 3.0 T. J Magn Reson Imaging 2014;39:1191–7.
[6] Kaiser J, Vignos MF, Liu F, Kijowski R, Thelen DG. American society of biomechanics clinical biomechanics award 2015: MRI assessments of cartilage mechanics, morphology and composition following reconstruction of the anterior cruciate ligament. Clin Biomech 2016;34:38–44.
[7] Li X, Kuo D, Theologis A, Carballido-Gamio J, Stehling C, Link TM, et al. Cartilage in anterior cruciate ligament-reconstructed knees: MR T1rho and T2-initial experience with 1-year follow-up. Radiology 2011;258:505–14.
[8] Andriacchi TP, Mundermann A, Smith RL, Alexander EJ, Dyrby CO, Koo S. A framework for the in vivo pathomechanics of osteoarthritis at the knee. Ann Biomed Eng 2004;32:447–57.
[9] Andriacchi TP, Mündermann A. The role of ambulatory mechanics in the initiation and progression of knee osteoarthritis. Curr Opin Rheumatol 2006;18:514–18.
[10] Anderst W, Zauel R, Bishop J, Demps E, Tashman S. Validation of three-dimensional model-based tibio-femoral tracking during running. Med Eng Phys 2009;31:10–16.
[11] Sheehan FT, Zajac FE, Drace JE. Using cine phase contrast magnetic resonance imaging to non-invasively study in vivo knee dynamics. J Biomech 1998;31:21–6.
[12] Kaiser J, Bradford R, Johnson K, Wieben O, Thelen DG. Measurement of tibiofemoral kinematics using highly accelerated 3D radial sampling. Magn Reson Med 2013;69:1310–16.
[13] d'Entremont A, Nordmeyer-Massner J, Bos C, Wilson D, Pruessmann K. A dynamic measurement method for knee biomechanics. In: Proceedings of the international society for magnetic resonance in medicine, ISMRM, Montreal, Quebec, Canada; 2011.
[14] Borotikar BS, Sheehan FT. In vivo patellofemoral contact mechanics during active extension using a novel dynamic MRI-based methodology. Osteoarthr Cartil 2013;9:1886–94.
[15] d'Entremont AG, Nordmeyer-Massner JA, Bos C, Wilson DR, Pruessmann KP. Do dynamic-based MR knee kinematics methods produce the same results as static methods? Magn Reson Med 2013;69:1634–44.
[16] Draper CE, Santos JM, Kourtis LC, Besier TF, Fredericson M, Beaupre GS, et al. Feasibility of using real-time MRI to measure joint kinematics in 1.5T and open-bore 0.5T systems. J Magn Reson Imaging JMRI 2008;28:158–66.
[17] Barrance PJ, Williams GN, Snyder-Mackler L, Buchanan TS. Altered knee kinematics in ACL-deficient non-copers: a comparison using dynamic MRI. J Orthop Res 2006;24:132–40.
[18] Asakawa DS, Pappas GP, Blemker SS, Drace JE, Delp SL. Cine phase contrast magnetic resonance imaging as a tool for quantification of skeletal muscle motion. Semin Musculoskelet Radiol 2003;7:287–96.
[19] Rebmann AJ, Sheehan FT. Precise 3D skeletal kinematics using fast phase contrast magnetic resonance imaging. J Magn Reson Imaging JMRI 2003;17:206–13.
[20] Barrance PJ, Williams GN, Novotny JE, Buchanan TS. A method for measurement of joint kinematics in vivo by registration of 3-d geometric models with cine phase contrast magnetic resonance imaging data. J Biomech Eng 2005;127:829–37.
[21] Pelc NJ, Drangova M, Pelc LR, Zhu Y, Noll DC, Bowman BS, et al. Tracking of cyclic motion with phase-contrast cine MR velocity data. J Magn Reson Imaging 1995;5:339–45.
[22] Meyer FG, Constable RT, Sinusas AJ, Duncan JS. Tracking myocardial deformation using phase contrast MR velocity fields: a stochastic approach. IEEE Trans Med Imaging 1996;15:453–65.
[23] Smith P. Development of the concepts of knee kinematics. Arch Phys Med Rehabil 2003;84:1895–902.
[24] Kato H, Kuroda M, Yoshimura K, Yoshida A, Hanamoto K, Kawasaki S, et al. Composition of MRI phantom equivalent to human tissues. Med Phys 2005;32:3199–208.
[25] Söderkvist I, Wedin P-Å. Determining the movements of the skeleton using well-configured markers. J Biomech 1993;26:1473–7.
[26] Barrance PJ, Williams GN, Buchanan TS. Design of a motion phantom for accuracy determination in the measurement of joint kinematics using cine phase contrast MRI data. In: Proceedings of the summer bioengineering conference., Key Biscayne, Florida; 2003.
[27] Van de Velde SK, Gill TJ, Li G. Evaluation of kinematics of anterior cruciate ligament-deficient knees with use of advanced imaging techniques, three--dimensional modeling techniques, and robotics. J Bone Jt Surg Am Vol 2009;91:108–14 suppl 1.
[28] Scanlan SF, Chaudhari AM, Dyrby CO, Andriacchi TP. Differences in tibial rotation during walking in ACL reconstructed and healthy contralateral knees. J Biomech 2010;43:1817–22.
[29] Tashman S. Abnormal rotational knee motion during running after anterior cruciate ligament reconstruction. Am J Sports Med 2004;32:975–83.
[30] Taylor KA, Terry ME, Utturkar GM, Spritzer CE, Queen RM, Irribarra LA, et al. Measurement of in vivo anterior cruciate ligament strain during dynamic jump landing. J Biomech 2011;44:365–71.
[31] Thorhauer E, Tashman S. Validation of a method for combining biplanar radiography and magnetic resonance imaging to estimate knee cartilage contact. Med Eng Phys 2015;37:937–47.
[32] Hosseini A, Van de Velde S, Gill TJ, Li G. Tibiofemoral cartilage contact biomechanics in patients after reconstruction of a ruptured anterior cruciate ligament. J Orthop Res 2012;30:1781–8.
[33] Behnam AJ, Herzka DA, Sheehan FT. Assessing the accuracy and precision of musculoskeletal motion tracking using cine-PC MRI on a 3.0T platform. J Biomech 2011;44:193–7.
[34] Fellows RA, Hill NA, MacIntyre NJ, Harrison MM, Ellis RE, Wilson DR. Repeatability of a novel technique for in vivo measurement of three-dimensional patellar tracking using magnetic resonance imaging. J Magn Reson Imaging 2005;22:145–53.
[35] Coleman JL, Widmyer MR, Leddy HA, Utturkar GM, Spritzer CE, Moorman CT III, et al. Diurnal variations in articular cartilage thickness and strain in the human knee. J Biomech 2013;46:541–7.
[36] Fukubayashi T, Kurosawa H. The contact area and pressure distribution pattern of the knee: a study of normal and osteoarthrotic knee joints. Acta Orthop 1980;51:871–9.
[37] Neu CP, Walton JH. Displacement encoding for the measurement of cartilage deformation. Magn Reson Med 2008;59:149–55.
[38] Chan DD, Cai L, Butz KD, Trippel SB, Nauman EA, Neu CP. In vivo articular cartilage deformation: noninvasive quantification of intratissue strain during joint contact in the human knee. Sci Rep 2016;6:19220.